Journal of Colloid and Interface Science 718 (2026) 140434

Contents lists available at ScienceDirect

Journal of Colloid And Interface Science

journal homepage: www.elsevier.com/locate/jcis

Swelling-state-dependent structure of spread microgel monolayers

T. Kratzenberg [a], Y. Gerelli [b,c,*], P. Gutfreund [d], P. Sánchez-Puga [d], A. V. Petrunin [a], W. Richtering [a,e], B. R. Thompson [f], A. Scotti [g,*]

[a] Institute of Physical Chemistry, RWTH Aachen University, Landoltweg 2, Aachen, D-52056, Germany
[b] Consiglio Nazionale delle Ricerche, Institute for Complex Systems, Piazzale Aldo Moro 2, Rome, ITA-00185, Italy
[c] Department of Physics, Sapienza University of Rome, Piazzale Aldo Moro 2, Rome, ITA-00185, Italy
[d] Institut Laue-Langevin, Avenue des Martyrs 71, Grenoble, FR-38042, France
[e] DWI-Leibniz Institute for Interactive Materials, Forckenbeckstr. 50, Aachen, D-52056, Germany
[f] Department of Chemical and Biomolecular Engineering, Center for Neutron Science, University of Delaware, Newark, DE 19716, Delaware, USA
[g] Division of Physical Chemistry, Lund University, Lund, SE-22100, Sweden

ARTICLE INFO

Keywords:
Microgels
Neutron reflectometry
Interfacial structure
Stimuli-responsive colloids

ABSTRACT

Albeit largely studied, the interfacial restructuring that governs emulsion breakdown remains poorly understood. Here, we use neutron reflectometry to probe the structure of thermo-responsive microgel monolayers formed either above the volume phase transition temperature or collapsed *in situ* after adsorption. We find that the thermal history of the microgel critically affects the monolayer architecture, particularly the particle protrusion into the air phase. These insights reveal a pathway-dependent mechanism that governs microgel behavior at interfaces, underpinning the design of next-generation responsive emulsions and interfacial materials.

1. Introduction

Microgel-stabilized emulsions have attracted increasing attention for their ability to break on demand in response to external stimuli such as temperature changes [1–5]. In the field of soft colloids, poly(*N*-isopropylacrylamide) (pNIPAM) microgels are among the most studied due to their well-defined thermoresponsive behavior near physiological conditions, as well as the scalability of their synthesis across various architectures and sizes [6–8]. The mechanical properties of these particles can be finely tuned, for example by varying crosslinker concentration during synthesis, yielding elastic moduli from a few to hundreds of kPa [9,10].

Both the thermoresponsiveness and the softness of the microgels play pivotal roles in determining emulsion stability and resistance to flocculation [11]. Recent studies have presented distinct, yet not mutually exclusive, strategies for generating monodisperse and not flocculated emulsions: some suggest using only very soft and highly deformable microgels, [11–14] while another proposes adsorbing microgels above their volume phase transition temperature (VPTT) and cooling them afterwards [15].

These observations underscore the pathway-dependent nature of microgel-stabilized emulsions, in which interfacial organization emerges from a complex interplay between particle properties, adsorption kinetics, and emulsification conditions such as concentration, droplet breakup, and coalescence dynamics. This complexity highlights that the adsorption history and interfacial restructuring of microgels are key, yet still insufficiently understood, determinants of emulsion destabilization in microgel-laden systems [16–18].

Several hypotheses have been proposed to explain destabilization above VPTT, including: (i) microgel desorption, (ii) changes in the structure orthogonal to the interface, (iii) in-plane rearrangements, (iv) alterations in the rheological properties of the interface, and (v) microgel aggregation or multilayer formation [12,19–25]. While earlier studies focused on desorption of microgels from the interface upon collapse, it is nowadays accepted that temperature or a change in particle volume do not significantly alter interfacial activity [25,26], making desorption an unlikely primary mechanism. Instead, structural changes within the microgel interfacial monolayer, both in-plane and out-of-plane, are now considered key contributors to emulsion instability. Collapse of the microgels from the aqueous phase onto the interface may introduce local stresses in the curved interface, facilitating its destabilization.

Different techniques have been used to study the interfacial behavior of microgels; however, most of them rely on *ex-situ* imaging (e.g., Cryo-SEM) [12,27], which can introduce artifacts due to drying or freezing, making the direct comparison with the original system extremely challenging [28–32].

Thus, more recent studies have focused on in-situ techniques to study the structural properties of microgel monolayers by employing small

* Corresponding authors.
E-mail addresses: yuri.gerelli@cnr.it (Y. Gerelli), andrea.scotti@chem.lu.se (A. Scotti).

https://doi.org/10.1016/j.jcis.2026.140434
Received 22 January 2026; Received in revised form 30 March 2026; Accepted 31 March 2026
Available online 7 April 2026

angle light scattering and specular as well as off-specular X-ray reflectivity [30,32,33].

However, investigations of effect of temperature on the structural properties of microgel monolayers remain limited. Out-of-plane structural changes above the VPTT have been observed by ellipsometry and neutron reflectometry, while atomic force microscopy has revealed changes in the interparticle, in-plane, interactions [24–26,34,35].

By performing numerical coarse-grained simulations, Kolker et al. [36] have shown that microgels deposited to the interface in a collapsed state can become kinetically trapped, adopting metastable morphologies that persist even upon swelling-deswelling cycles, leading to interfacial hysteresis in shape and size [36]. This underlines the importance of exploring how the adsorption pathway governs interfacial microgel architecture experimentally.

Neutron reflectometry (NR) offers a non-destructive method to probe *in-situ* the internal structure of interfacial layers with sub-nanometer resolution [37,38]. Recent advances in data modeling and experimental design have thus provided a foundation for the *in-situ* investigation of microgel monolayers above and below their VPTT [34], and at different concentrations [39].

In this work, we investigate the structural evolution of pNIPAM microgel monolayers at the air-water interface above their VPTT at different surface concentrations using neutron reflectometry. We compare two pathways: (i) direct spreading at 40 °C of collapsed microgels followed by compression; and (ii) spreading of swollen microgels at 20 °C, followed by compression and heating to 40 °C (collapse).

Our results reveal pathway-dependent differences in monolayer structure, particularly in the extent of microgel protrusion into the air phase and the polymer density at the interface. These features may play a crucial role in destabilizing the curved interfaces of emulsions and will help to understand the mechanisms governing the temperature induced breakdown of emulsions stabilized by thermoresponsive microgels.

2. Materials and methods

2.1. Microgel synthesis

For the synthesis of the microgels, 1.2565 g of D7-N-Isopropylacrylamide (NIPAM) ($C_6H_4D_7NO$), 0.0801 g of N,N'-Methylenebis(acrylamide) (BIS) and 0.0293 g of sodium dodecyl sulfate (SDS) were dissolved in 62 mL double-distilled water that was filtered through a 0.2 μm syringe filter. The solution was brought to 70 °C in a three-neck 100 mL flask. Potassium persulfate (KPS) (0.0274 g) was dissolved in 3 mL of the same double-distilled water. Both solutions were bubbled with nitrogen for 60 min, after which the reaction was started by adding the KPS into the flask. The reaction mixture was kept at 70 °C under nitrogen flow for 4 h. The microgels were purified by four-fold ultracentrifugation at 30.000 rpm followed by redispersion in fresh double-distilled water. They were lyophilized for storage.

The use of partially deuterated NIPAM was necessary to increase the signal originating from the microgel monolayer in the neutron reflectometry experiments. The microgel particles obtained with this protocol are characterized by a 5 % cross-linker concentration and by a hydrodynamic radius of $R_{20°C} = (126 \pm 2)$ nm.

2.2. Compression isotherms

Langmuir monolayers consisting of microgels were prepared at the air-water interface using a custom-made Langmuir-Blodgett trough made of poly(oxymethylene)glycol with a total area of approximately 402 cm^2, equipped with a pressure sensor and a motorized dipper (KSV NIMA, Biolin Scientific Oy, Finland) [26]. The liquid phase consisted of Milli-Q water with a conductivity of 60 μS cm^{-2}. A paper Wilhelmy plate (l = 20.6 mm) was used to measure the surface pressure. Investigations of the microgels were carried out at the water-air rather than at the water-oil interface to improve the signal-to-noise ratio in NR experiments. Moreover, earlier studies have revealed only minor differences between the interfacial behavior of microgels at these two interfaces [35,40,41].

Prior to each measurement, the trough was thoroughly cleaned with ethanol and Milli-Q water, and a clean air-water interface was prepared. The temperature of the liquid phase was controlled using a circulation water bath. Microgel dispersions (10 mg mL^{-1} in D_2O) were mixed with 50 vol% isopropanol to promote spreading at the interface. For experiments at 20 °C, the solution was applied dropwise at room temperature using a Hamilton syringe. For experiments at 40 °C, both the syringe and the microgel solution were pre-heated above 40 °C to ensure that the microgels were collapsed upon spreading.

After an equilibration time of at least 30 minutes, the surface area was compressed at a constant rate of 6.48 cm^2 min^{-1} to a target surface area of 42 cm^2.

2.3. Langmuir-Blodgett gradient depositions

For performing atomic force microscopy (AFM) measurements, Langmuir-Blodgett gradient depositions were performed to transfer the microgel monolayer from the air-water interface to the surface of a silicon wafer. Each silicon substrate was cleaned twice in an ultrasound bath with isopropanol and subsequently ozone-treated for 15 minutes (UVC-1014, NanoBioAnalytics, Germany). It was then mounted on a custom-made holder and immersed into the subphase at an angle of approximately 25° relative to the air-water interface. Microgel monolayers were formed as described in the previous section. After the spreading, and formation of the monolayer, the compression was started and the substrate was withdrawn simultaneously vertically from the interface at a speed of 0.15 mm min^{-1} thus enabling the formation of a gradient deposition on the wafer surface. The transferred monolayer was then imaged using AFM.

2.4. AFM imaging

AFM images of microgel films in the dry state were recorded with either a Dimension Icon (Veeco Instruments Inc, USA, Nanoscope 9.4, Bruker Co., USA) or a Nanowizard 3 (JPK Instruments AG, Germany, Bruker Co., USA), both operated in closed-loop mode. Imaging of microgel monolayers was performed in tapping mode with OTESPA tips (NanoAndMore GmbH, Germany) with a nominal spring constant of 26 mN m^{-1}, a nominal resonance frequency of 300 kHz and a nominal tip radius of 7 nm. For phase imaging of separate microgels, OLTESPA tips (Bruker Co., USA) with a nominal spring constant of 2 mN m^{-1}, a nominal resonance frequency of 70 kHz and a nominal tip radius of 7 nm were used. In this case, a cantilever with a lower stiffness was chosen to increase the drive amplitude to maximize the contrast in the phase images. All images were recorded with a scan size of 5×5 μm^2 with a resolution of 512×512 pixels. Images were processed using the open-source software Gwyddion [42]. The area per particle A_p and the nearest neighbour distances (NNDs) in the monolayers were determined using a custom MATLAB routine (MathWorks Inc, USA) based on the particle tracking algorithm by CROCKER and GRIER [26,43,44].

Height profiles were obtained from linear interpolation of height data parallel and perpendicular to the AFM fast-scan direction respectively. The average height profile was then obtained by averaging over at least 120 individual microgels.

2.5. Neutron reflectometry

Neutron reflectometry experiments were carried out at the air-water interface on the time-of-flight FIGARO reflectometer at the Institut Laue-Langevin (ILL, Grenoble, France) [45]. A Teflon Langmuir trough (705 cm^2, Nima Technology Ltd., United Kingdom) was used for all measurements and enclosed in a temperature-controlled chamber equipped

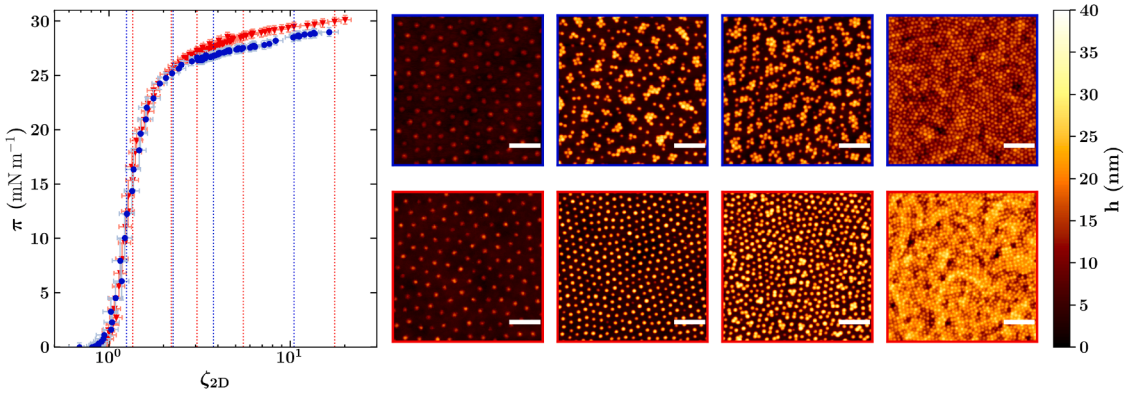

Fig. 1. Phase behavior of the microgel monolayers. (left) Compression isotherm of D7-pNIPAM microgels recorded at 20 °C (swollen microgel, blue) and at 40 °C (collapsed microgel, red) at the air-water interface. The vertical dotted lines indicate the surface pressures measured during neutron reflectometry experiments. Red lines represent measurements performed with collapsed microgels above the VPTT. Blue lines show measurements with swollen microgels. (right) Example AFM height images of microgel monolayers at the solid-air interface with increasing ζ_{2D} (Equation 1) from left to right deposited at 20 °C below the VPTT (top, blue frames) and at 40 °C above the VPTT (bottom, red frames). The white scale bars are 1 μm in size. (For interpretation of the references to colour in this figure legend, the reader is referred to the web version of this article.)

with sapphire windows to minimize evaporation and allow neutron transmission.

In order to maximize the signal of the microgels, air contrast matched water (ACMW) was used instead of water as liquid subphase. ACMW is a mixture of D_2O and H_2O (8:92, v/v %) with a null scattering length density (SLD) that matches that of air ($SLD_{air} = 0$ Å^{-2}) [46]. For this reason it is also refereed to as null-reflecting water since a clean air-ACMW interface does not generate any reflectivity signal. The trough was thoroughly cleaned before each experiment, and a neat interface was prepared before every measurement.

Microgels dispersed at 10 mg mL^{-1} in D_2O were mixed 1:1 (v/v) with isopropanol to facilitate the spreading of the drop-casted microgel suspension at the interface. For microgels adsorbed at 20 °C, the solution was drop-casted at 20 °C using a Hamilton syringe. The surface area was then compressed until the target surface pressure was reached and finally the temperature was increased to 40 °C. For microgels adsorbed at 40 °C, the Hamilton syringe, the microgel suspension, and the aqueous phase were pre-heated at 40 °C to ensure that the microgels were in the collapsed state during spreading. In both cases, compression was performed symmetrically at a constant rate of 6.48 cm^2 min^{-1}.

NR data were collected in time-of-flight mode with wavelengths ranging from $\lambda_0 = 2$ Å to $\lambda_0 = 20$ Å at incident angles $\theta_1 = 0.717°$ and $\theta_2 = 3.878°$, corresponding to a Q-range from approximately 0.1 to 4 nm^{-1}. In this context, Q refers to the wave-vector transfer in air and it can be calculated using $n = 1$ and $\theta = 2\theta_1$ and $\theta = 2\theta_2$ in Equation S1. In the context of specular NR, the wave-vector transfer is parallel to the normal direction to the interface, z, and therefore $Q \equiv Q_z$. The beam footprint was maintained at 80×45 mm^2. Reflected neutrons were detected using a 2D ^{3}He detector, and the data were reduced to reflectivity $R(Q)$ using the COSMOS routine. Reflectivity curves can be displayed in different scales, according to the features to be highlighted. In the case of microgel monolayers, and as previously reported by us [39], the most informative representation of the reflectivity data is obtained by plotting $R(Q) \times Q^2$ versus Q on a log-log scale. This approach enhances the visibility of both low-Q features, which are sensitive to the overall thickness of the microgel monolayer, and high-Q features, which reflect its internal architecture.

3. Results

3.1. Phase behavior of the microgel monolayers

To unravel the influence of the microgel volume phase transition on the stability of the interface, we probed the structure of monolayers formed at the air-water interface by adsorbing: (i) collapsed microgels above the VPTT, i.e. at 40 °C, that are then compressed laterally at the desired surface pressure; (ii) swollen microgels that are first compressed at the desired surface pressure and then collapsed at the interface by raising the temperature above the VPTT.

A detailed account of the samples used and of the experiments performed are provided in the Materials and methods section and in the ESI, together with the description of the experimental techniques exploited. For all experiments, the same microgels (D7-pNIPAM) were used; they were synthesized with a nominal 5 mol% cross-linker concentration obtained starting from a partially deuterated monomer with 7 atoms of deuterium, $C_6D_7H_4NO$. The VPTT for this microgel in solution is $\approx 32 - 33$ °C as confirmed by the dependence of the hydrodynamic radius on temperature, determined by multi-angle dynamic light scattering (DLS) (Figure S1). At 40 °C, the microgel hydrodynamic radius was 60.2±0.8 nm leading to a swelling ratio of 2.09±0.05 defined as the ratio between the hydrodynamic radius of the swollen and the collapsed microgel [8].

In analogy with the generalized volume fraction used to describe the microgel concentration in bulk suspensions [47], we introduce the two-dimensional compression parameter ζ_{2D} [26] to quantify the lateral crowding of microgels at the interface:

$$\zeta_{2D} = \frac{A_{P,0}}{A_P}, \tag{1}$$

where $A_{P,0}$ is the area occupied by an isolated, uncompressed microgel at the interface, and A_P is the area per microgel in the compressed monolayer. $A_{P,0}$ is determined from AFM phase images of single microgels and A_P from microgel deposited at different surface pressures (see ESI, Section 2.4). ζ_{2D} as a dimensionless parameter provides a direct measure of the lateral compression experienced by the monolayer: $\zeta_{2D} = 0.90$ corresponds to the dilute limit of non-interacting particles, describing the ratio between the area occupied by a particle with radius R and the area per particle for ideally hexagonally packed particles with an interparticle distance of $2R$. Higher values indicate increasing particle crowding and overlap. Because ζ_{2D} is based on in-plane geometrical considerations and it is independent of the vertical structure, it serves as a convenient and reproducible control parameter for comparing different monolayer states. Notably, ζ_{2D} is not defined based on the total nominal spread amount, as some particles can be lost to the subphase, particularly in the collapsed state. This makes the definition a reliable indicator of the actual interfacial compression. Further, while the 2D-structure of a microgel monolayer can be affected by the deposition process [30,32], the averaged area per particle A_P is independent of local structural changes assuming no changes in concentration.

The compression isotherms of D7-pNIPAM microgels at the air-water interface exhibit the characteristic features to those previously reported for fully hydrogenated microgels ($[C_6H_{11}NO]_n$) with a core-corona structure (see Figs. 1 and S3) which are five distinct isotherm regimes related to a structural transition of the microgels [44].

Compression isotherms performed at 40 °C show a surface pressure evolution qualitatively similar to that observed at 20 °C (see Fig. S3), but the onset of monolayer formation, marked by the rise in surface pressure, occurs at a slightly higher particle density. This shift is attributed to the reduced lateral spreading of the microgels when they are adsorbed in a collapsed state [26]. This is not surprising, as each collapsed particle occupies a smaller interfacial area, requiring a higher surface concentration to achieve full coverage, delaying the formation of a contiguous monolayer (see Fig. S5) [44]. Thus, when surface pressure π is plotted against ζ_{2D} the isotherms recorded below and above the VPTT superimpose at low surface pressure as ζ_{2D} accounts for the lower interfacial coverage of the microgels above the VPTT. Unlike in the swollen state, since the microgel core is already collapsed, no second plateau at $\zeta_{2D} \gtrsim 7$ in the surface pressure is observed upon further compression (see red triangles and blue circles in Fig. 1). The second plateau is originated from the compression of the soft corona surrounding a more rigid core [44]. Indeed, small-angle X-ray scattering measurements of the microgel form factor in diluted suspensions shows that, above the VPTT, the particles are completely collapsed and exhibit homogeneous, compact structure, eliminating this compressibility contrast (Fig. S2). As a result, the surface pressure increases steadily until the monolayer ultimately collapses at high compression.

3.2. Collapsed microgels adsorbed above the VPTT

In NR experiments, collapsed microgels were spread at the air-water interface kept at 40 °C and the resulting monolayer was then compressed to the target ζ_{2D} values of 1.35, 2.21, 3.06, 6.12 and 17.6, corresponding to surface pressure π values of 15.3, 25.5, 28.8, and 30.0 mN m^{-1}. The corresponding NR data are shown in Fig. 2. As described in the Materials and Methods section, for an optimal representation, reflectivity data are plotted as $R(Q) \times Q^2$.

Notably, as ζ_{2D} increases, the reflectivity curves exhibit progressively higher and higher intensity in the intermediate Q-range (2×10^{-1} nm$^{-1} \lesssim Q \lesssim 6 \times 10^{-1}$ nm^{-1}). This is due to a greater average polymer content within the illuminated region. The variations in the reflectivity fringes for $Q \lesssim 2 \times 10^{-1}$ nm^{-1} are instead caused by differences in the film structure across the different states of compression.

The reflectivity curves in Fig. 2A at $\zeta_{2D} = 3.06$ (■) and $\zeta_{2D} = 6.12$ (★), both corresponding to compression states shortly after the onset of the plateau in the $\pi(\zeta_{2D})$ isotherm (Figs. 1 and S3B), deviate from the trend observed at lower concentrations, as they appear nearly identical. This suggests a temporary saturation in the structural response of the monolayer under compression.

At the highest surface concentration ($\zeta_{2D} = 17.6$), the reflectivity increases again at low Q (compare ○ and ⬟ in Fig. 2A) more directly reflecting the significantly larger microgel density located at the interface. Moreover, the appearance of a larger number of more pronounced fringes in the $R(Q)$ at this concentration indicates an increase in the overall thickness of the interfacial film. These variations in reflectivity are quantitatively captured by the fitted polymer volume fraction profiles $\phi(z)$ (Fig. 2B), which offer structural insight into the monolayer organization across compression states.

All volume fraction profiles (VFPs) share characteristic structural features: a well-defined, polymer-rich region onto the air-water interface (peaking at $z = 0$ nm), a limited protrusion into the air phase ($z < 0$), and a more extended tail into the aqueous subphase ($z > 0$). This asymmetry is consistent with the hydrophilic nature of pNIPAM, which swells in water but collapses in the poor-solvent environment of the air, and with the opposing influence of interfacial tension, which penalizes protrusion into the air.

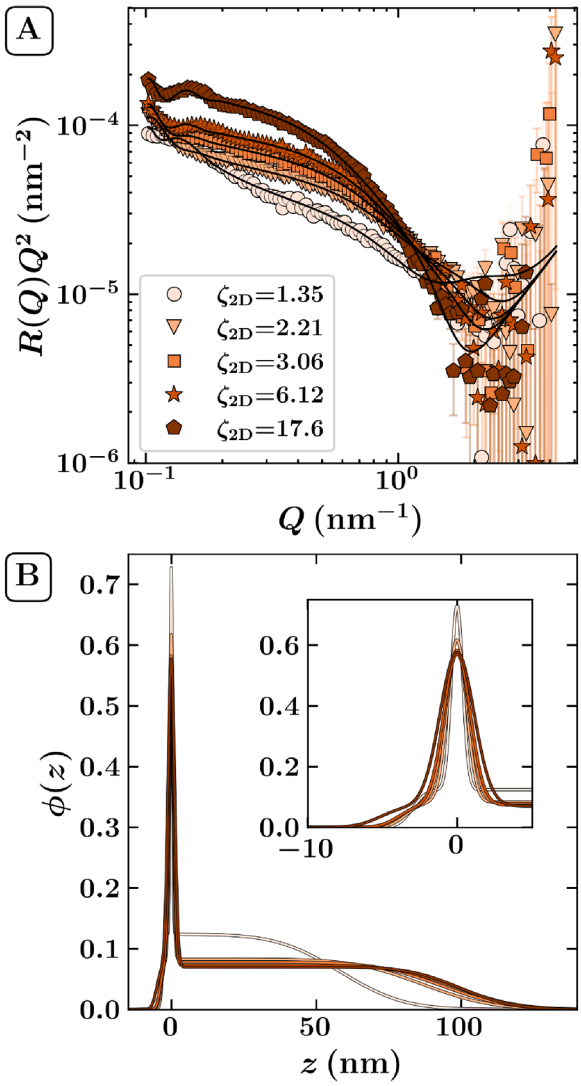

Fig. 2. Collapsed microgels adsorbed and then compressed. (A) Neutron reflectivity data (symbols) for monolayers formed from collapsed microgels adsorbed and compressed at 40 °C. Product of the reflectivity R with the square of the wavevector Q plotted against Q. The different compression states correspond to the ζ_{2D} values indicated in the legend. Model fits to the data are shown as solid black lines. (B) Polymer volume fraction profiles $\phi(z)$ corresponding to the fits shown in panel A, obtained by inverting Equation S5. The profiles are plotted as a function of z, the distance from the air-water interface (defined as $z = 0$ nm). Each $\phi(z)$ curve shares the same color as the corresponding experimental dataset (symbols) in panel A.

At the lowest surface concentration (▭), the VFP differs markedly from those at higher compression. Their vertical extension (along z) and the narrow width of the interfacial peak suggest that microgels are laterally spread and vertically compressed, and, very likely, adopting the characteristic "fried-egg" morphology observed in earlier studies of microgel monolayers at interfaces [48,49]. In this configuration, despite being at a temperature higher than the VPTT, the loosely crosslinked outer corona flattens at the interface to reduce interfacial energy, while the denser core remains compact and contributes modestly to the overall profile. Therefore, in the dilute regime the in-plane spreading of the microgel is maximized causing a contraction of the microgels in the out-of-plane direction. Quantitatively, the model suggests that the Gaussian component of $\phi(z)$, which captures the laterally diffuse chain layer at the interface, covers roughly 60% of the total interface, while the denser core contributes approximately 12% (equation S6). This reflects a struc-

ture dominated by adsorbed corona chains rather than by the compact microgel core. This ratio is slightly higher in the AFM data where the total area coverage of the microgel core is approximately 30% (compare Fig. S7). However, this can be attributed to greater lateral spreading of the microgel core due to a more pronounced vertical deformation on the solid substrate as compared to the gaseous phase as well as the difference in the adsorption kinetics. Attempts to model reflectivity using a solid-sphere approach, as applied for rigid particles at interfaces [37], failed to reproduce the data (see Fig. S9). This underscores the need for a model that accounts for microgel deformability, vertical gradients in polymer density, and corona spreading at the interface.

As ζ_{2D} increases to 2.21, 3.06, and 5.51, the VFP undergoes progressive restructuring. Starting from the air phase, the protrusion into the air phase (z_a) increases from 4.5 nm to 6.4 nm (Fig. 4A). Simultaneously, the peak height decreases by about 25%, while the interfacial width (w_i, Fig. 4B), that is the layer of polymer sitting directly onto the interface, increases from 6.5 nm to 9.5 nm. For what concern the protrusion into the aqueous subphase, z_w increases from 100 nm to 140 nm (Fig. 4C). This reflects a redistribution of the polymer from a narrow, high-density interface to a more diffuse, vertically extended structure. The decrease in peak amplitude is thus not due to loss of polymer but to redistribution of the same material over a broader vertical range.

These changes likely arise from increased interparticle repulsion and steric constraints at higher surface coverage. Since the microgels are already collapsed, further deswelling is not expected; instead, the monolayer accommodates compression through vertical expansion and interpenetration of neighboring corona regions. This out-of-plane deformation relieves lateral stress and increases the effective thickness of the interfacial layer, as also evidenced by the increased number and contrast of the fringes observed in the reflectivity at higher ζ_{2D} (see Fig. 2A).

Going to the highest surface concentration ($\zeta_{2D} = 17.6$), the reshaping becomes even more pronounced. The interfacial width exceeds 10 nm, and both z_a and z_w reach their maximum observed values for the monolayer formed by adsorbing collapsed microgels (Fig. 4). As supported by AFM images (Fig. S6) this behavior suggests the onset of core-core interactions and possible deformation of the inner microgel polymeric network.

The structural evolution of the microgel monolayer is closely reflected in the corresponding changes in surface pressure, particularly at higher surface concentrations. For instance, increasing ζ_{2D} from 1.35 to 2.21 leads to a substantial rise in surface pressure from 15.3 mN m^{-1} to 25.5 mN m^{-1} (see Fig. 1). This coincides with a pronounced increase in the microgel protrusion into the air phase (z_a), as revealed by the VFP analysis and in Fig. 4A. Such vertical expansion into air suggests a change in the microgel contact angle at the interface, likely driven by compression-induced reorganization of the corona. The increased interaction between microgels may force a greater portion of the core to reside closer to the interface or even partially enter the air phase, contributing to the observed increase in surface pressure.

Beyond this point, from $\zeta_{2D} = 2.21$ to 5.51, the structural changes primarily involve increased protrusion into the aqueous subphase (z_w in Fig. 4C), while the interfacial peak remain nearly constant. Despite the increase in microgel surface concentration, the surface pressure rises only from 25.5 to 28.5 mN m^{-1} (see Fig. 1). This plateau-like behavior in the isotherm suggests that further lateral compression is accommodated through vertical expansion into the water phase, without significant additional mechanical resistance at the interface.

3.3. Swollen microgels adsorbed below the VPTT and then collapsed at the interface

Swollen microgels were spread at the air-water interface at 20 °C and the resulting interfacial film was then compressed to the target ζ_{2D} values of 1.25, 2.26, 3.78, and 10.5, corresponding to surface pressure π values of 15.5, 25.5, 27.0, and 28.6 mN m^{-1}. Before starting the NR measurements and only after compression, the temperature of the interface was raised to 40 °C promoting the collapse of the microgels portion in the water subphase. The positions of the barriers were however kept constant, so that the particle density did not change. The corresponding NR data are shown in Fig. 3A.

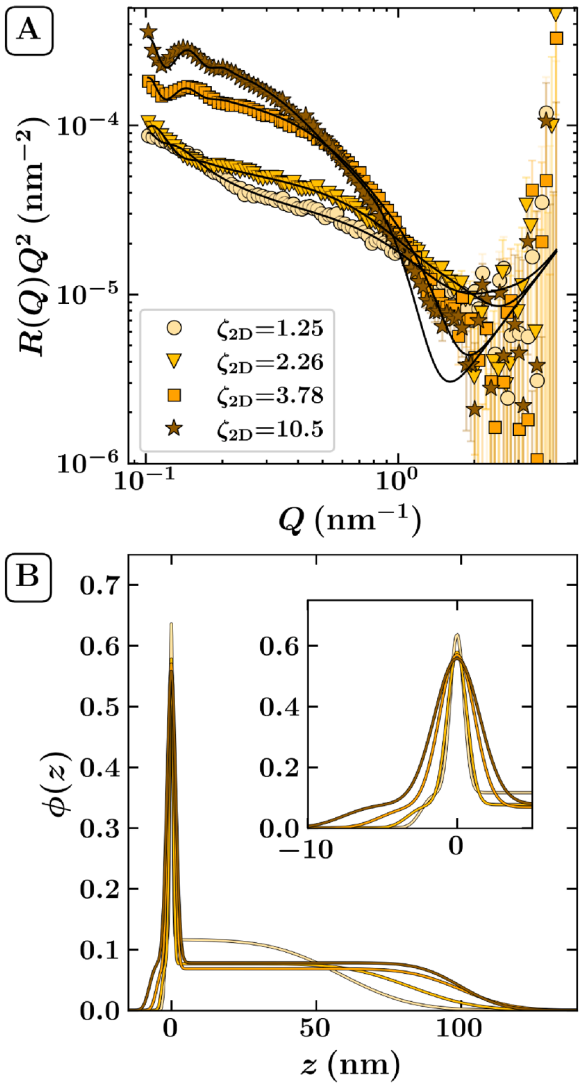

Fig. 3. Swollen microgels adsorbed, compressed, and then collapsed. (A) Neutron reflectivity data (symbols) for monolayers formed from swollen microgels adsorbed at 20 °C, compressed to the surface pressure of interest, and then heated to 40 °C prior to the measurement. The different compression states correspond to the ζ_{2D} values indicated in the legend. Model fits to the data are shown as solid black lines. (B) Polymer volume fraction profiles $\phi(z)$ corresponding to the fits shown in panel A, obtained by inverting equation S5. The profiles are plotted as a function of z, the distance from the air-water interface (defined as $z = 0$ nm). Each $\Phi(z)$ curve shares the same color as the corresponding experimental dataset (symbols) in panel A.

At first glance, the reflectivity curves for the microgels adsorbed at 20 °C, compressed, and subsequently collapsed appear similar to those recorded for the monolayers formed by microgels adsorbed in their collapsed state and then compressed. However, while both systems show comparable reflectivity values at very low Q in the lowest compression states, $R(Q \to 0)$ increases more significantly for the originally swollen microgels than for their collapsed counterparts. Given that $R(Q \to 0)$ is directly related to the total scattering length per unit area, when using air-contrast matched water in the subphase, this trend indicates a higher total polymer content in the interfacial region [50].

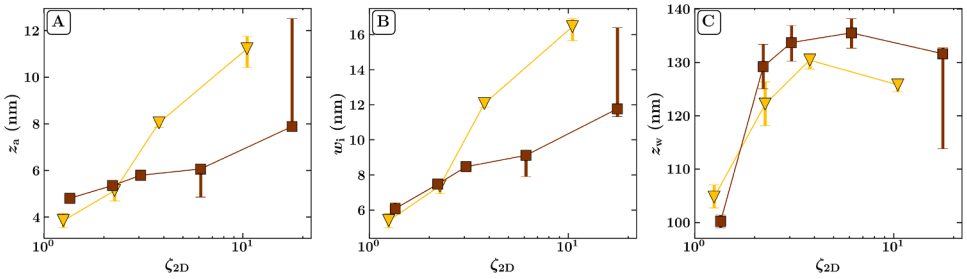

Fig. 4. Monolayer reorganization. Structural parameters extracted from the analysis of neutron reflectivity data for monolayers composed of collapsed microgels (brown squares) and swollen-then-collapsed microgels (yellow triangles). All measurements were performed at 40 °C. Plotted as a function of the compression parameter ζ_{2D} are: (A) the protrusion into the air phase, z_a; (B) the width of the monolayer at the interface w_i calculated from z_a and the width of the amplitude W_g; and (C) the protrusion into the aqueous subphase, z_w. (For interpretation of the references to colour in this figure legend, the reader is referred to the web version of this article.)

In addition to the increased microgel protrusion into the aqueous subphase, the polymer VFPs in Fig. 3B reveal significant structural changes in the immediate vicinity of the interface as a function of compression. For the swollen-then-collapsed microgels, the protrusion into the air phase increases with ζ_{2D}: $z_a \approx 4$ nm at the lowest surface concentration, reaching approximately $z_a \approx 11$ nm at the highest.

Concurrently, the extension of the interfacial polymer-rich region, quantified by W_g, the width of the Gaussian component in Equation S6, also increases with compression. While W_g is relatively narrow at low ζ_{2D}, it broadens substantially as the microgels are compressed, indicating progressive reorganization of polymer chains at the interface. This behavior reflects the enhanced lateral crowding experienced during compression.

3.4. Comparison of the collapsed microgel structures

While all the measured monolayers ultimately contain collapsed microgels at the interface, the route taken to achieve this final state has a pronounced impact on the molecular organization, vertical distribution, and surface excess of the polymer. These differences are evident in the extracted volume fraction profiles, in the compression isotherms, and in the AFM images taken on dry deposited monolayers. They reflect the interplay between thermoresponsive collapse, interfacial deformation, and lateral interactions during film formation. Some of the parameters directly obtained from the modeling of NR data are compared in Fig. 4 for the two cases reported here (see also Table S3 for the full list of NR-derived parameters).

For both adsorption pathways, the protrusion of the microgels into the air (z_a) and the width of the interfacial polymer-rich region (w_i) increase with lateral compression (Fig. 4A, and B). At low surface concentration, both parameters are small and comparable between the two systems. However, in the intermediate compression regime ($\zeta_{2D} > 3$), a clear divergence emerges: for adsorbed-swollen-then-collapsed microgels (triangles), both z_a and w_i increase more rapidly with compression than in the monolayer formed by adsorbing collapsed microgels (squares).

Interestingly, this divergence seems to be correlated with the differences observed for $\zeta_{2D} \gtrsim 2$ in the compression isotherms measured below and above the VPTT (Fig. S3). This might indicate a different packing of the microgel corona under compression.

Furthermore, this difference indicates distinct interactions between polymer chains within the microgel coronas adsorbed at the interface. When microgels are adsorbed in the swollen state, microgel coronas are extended and can interpenetrate, leading to variations in the structure at the interface at sufficiently high microgel concentrations. The inflection observed in the compression isotherm can be interpreted as the onset of a two-dimensional phase transition within the Langmuir film that might be accompanied by a progressive clustering process. AFM images of transferred films formed from swollen microgels (Fig. 1) support this scenario, revealing microdomains in the deposited dry film indicative of local aggregation driven by corona interpenetration and chain entanglement. Whether these clusters are also present at the air-water interface is still debated as they might be a consequence of the monolayer deposition onto a solid substrate [30,51].

Upon temperature-induced collapse, the presence of interpenetrated coronas leads to a higher total polymer content at the interface compared to the case of the monolayer formed by collapsed microgels, as evidenced by the more pronounced increase in $R(Q \to 0)$ with compression. By contrast, despite clear deformation and chain spreading at the interface, adsorbed collapsed microgels exhibit a steric repulsion between particles, consistent with hard-sphere-like behavior. This is confirmed by the ordering seen in AFM images of the dry monolayer, which reflects lateral exclusion and, therefore, the absence of interpenetration and of the attractive term during deposition that leads to the pronounced clustering in the case of the monolayer formed by swollen microgels that are then collapsed.

Above the VPTT, the surface tension is slightly lower than at 20 °C leading to reduced capillary interactions, and, as the microgel cores collapse during drying, their adhesion to the substrate is likewise expected to decrease [52]. As a lower adhesion to the substrate would promote clustering of the microgels [53], a reduction in capillary interactions would likewise inhibit the formation of clusters during the drying process. However, the divergence in the polymer structure at higher microgel concentrations indicates, that the delayed cluster formation might be related to a difference in the lateral microgel-microgel interactions. These observations suggest that, in the collapsed state, polymer chains preferentially reorganize to maximize interaction with the hydrophobic phase (air) [54], while swollen coronas promote local bridging or entanglement, ultimately altering the compression response of the film.

For microgels adsorbed at 40 °C, the width of the monolayer at the interface w_i is smaller at high microgel concentration than in the adsorbed-swollen-then-collapsed case (Fig. 4B ■), suggesting that the polymer directly adsorbed to the interface adopts a broader profile if the microgel is collapsed after the compression of the interface. This behavior indicates a different reorganization of the polymer content within the polymer rich interface, caused by the difference in the structure of the swollen and collapsed monolayer during the compression and prior to the NR experiments.

At 20 °C, microgels adsorb in a swollen state and flatten at the interface to minimize interfacial energy. This spreading is limited by network elasticity, leading to the characteristic “fried-egg" morphology [48,49]. When the temperature is increased after adsorption, the corona cannot fully desorb due to a combination of interfacial tension and poor solvent conditions, effectively freezing in place part of the extended polymer network. This behavior contrasts with the case of monolayer formed by adsorbed collapsed microgels, where spreading is hindered already at the adsorption stage due to both elastic resistance and limited chain mobility in the collapsed state. Thus more of the microgel denser core

is exposed to the interface to achieve a higher interfacial coverage. This explains the variances in the maximum protrusion in air z_a that depends on the adsorption path, while the width of the polymer film w_i in both experiments remains similar at low values of ζ_{2D}.

3.5. Comparison of the swollen and collapsed microgel structures

NR measurement series recorded at 20 °C for microgels adsorbed at 20 °C or 40 °C (Fig. S12) show a reduction of the protrusion in air z_a with increasing ζ_{2D}, in agreement with recent studies [39]. This behavior is opposite compared to the case of the collapsed monolayers for which z_a increases. Further, there exists a sudden increase in z_a at the highest value for ζ_{2D} suggesting that z_a passes through a minimum before it increases again close to the fourth compression regime (Fig. S12 A and B, compare Fig. S3).

Unlike for the collapsed microgels, the protrusion of the microgels in water z_w further increases for the swollen monolayers above $z_w \approx 3$ as the microgel core is further laterally compressed (Fig. S12 D). This indicates a higher deformability of the microgels due to the swollen microgel core and a softer network response [24,35].

These results emphasize that both the structure of the microgels corona adsorbed to the interface and the microgel core in the water subphase change as function of microgel concentration, temperature and thermal history.

4. Conclusion

The results presented here offer new mechanistic insight into how the thermal history of responsive microgels govern the interfacial architecture of soft particle monolayers. This has direct implications for the rational design of stimuli-responsive Pickering emulsions, where stability and destabilization must be precisely controlled.

Our findings demonstrate that microgels which are adsorbed to the interface in a swollen state and subsequently collapsed undergo a markedly different interfacial reorganization compared to microgels that adsorb in a collapsed form. Specifically, we show that swollen-then-collapsed microgels retain an extended corona structure upon collapse due to the kinetic trapping of chains at the interface. This leads to stronger particle-particle interactions, potentially forming interfacial clusters or networks that enhance mechanical integrity.

In contrast, collapsed microgels behave more like deformable soft spheres with steric repulsion and less interfacial entanglement, resulting in monolayers that are more compressible and less cohesive under stress.

These differences are not just structural but functionally significant: they determine the ability of the monolayer to resist coalescence, respond to environmental changes, and ultimately control emulsion stability.

In practical terms, the results suggest that emulsions stabilized by microgels adsorbed below the VPTT could be engineered to remain stable under mild conditions but break upon heating, as thermal collapse modifies both the individual particle structure and their lateral interactions. Conversely, if microgels are collapsed prior to adsorption, they form films that are less prone to network formation and thus more susceptible to rupture under external triggers such as pH, ionic strength, or mechanical shear.

The structural changes of the monolayers for the different spreading conditions underscore the need for additional studies investigating differences in microgel-microgel interactions to be measured e.g. by optical tweezers, AFM or interfacial rheology, in order to gain a comprehensive understanding of how these structural changes impact emulsion stability.

These insights contribute to a growing body of work that seeks to move beyond empirical emulsion stabilization toward predictive control based on interfacial microstructure. In particular, the ability to tune the interfacial connectivity and cohesion via the adsorption-collapse sequence offers a new design lever for developing emulsions that are robust under storage but breakable on demand, a feature central to applications in drug delivery, food science, and smart formulations.

Furthermore, the *in-situ* structural information can help in further developing computer simulations able to finally measure the stresses rising between microgels due to the collapse. For instance, similarly to what has been done in bulk [55], one can think to use two *in silico* microgels confined to the interface [49,56,57] to measure the force acting between them once the portion of the particle in the water subphase is collapsed and also varying the curvature of the interface where they are confined to finally measure the stress rising at the interface deriving by the structural variation of the monolayer.

CRediT authorship contribution statement

T. Kratzenberg: Writing – review & editing, Visualization, Validation, Investigation, Formal analysis, Data curation; **Y. Gerelli:** Writing – review & editing, Writing – original draft, Validation, Software, Data curation; **P. Gutfreund:** Writing – review & editing, Investigation, Data curation; **P. Sánchez-Puga:** Writing – review & editing, Investigation; **A. V. Petrunin:** Writing – review & editing, Investigation, Data curation; **W. Richtering:** Writing – review & editing, Funding acquisition; **B. R. Thompson:** Writing – review & editing, Investigation; **A. Scotti:** Writing –review & editing, Writing – original draft, Validation, Supervision, Resources, Project administration, Methodology, Investigation, Funding acquisition, Formal analysis, Conceptualization.

Data availability

Neutron reflectometry measurements have been performed at the Institut Laue Langevin under proposal number 9-10-1855 using the instrument FIGARO and the data are available at http://doi.ill.fr/10.5291/ILL-DATA.9-10-1855.

Declaration of competing interest

The authors declare the following financial interests/personal relationships which may be considered as potential competing interests: Andrea Scotti reports financial support was provided by Knut and Alice Wallenberg Foundation. Andrea Scotti reports financial support was provided by Swedish Research Council. Walter Richtering reports financial support was provided by Deutsche Forschungsgesellschaft. If there are other authors, they declare that they have no known competing financial interests or personal relationships that could have appeared to influence the work reported in this paper.

Acknowledgments

AS acknowledge financial support from the Knut and Alice Wallenberg Foundation (Wallenberg Academy Fellows) and from the Swedish Research Council (Research grant 2024-04178). T.K., A. V. P., W. R. and A. S. acknowledge financial support from the Deutsche Forschungsgesellschaft within project SFB985 “Functional Microgels and Microgel Systems”. B.R.T. acknowledges support from the NIST Center for Neutron Research under cooperative agreement no. 70NANB20H133. The partially deuterated NIPAM monomer has been produced by the deuteration user service at Jülich Centre for Neutron Science. We acknowledge the Institut Laue-Langevin for provision on neutron beamtime and the MAX IV Laboratory for beamtime on the coSAXS beamline under proposal 20240049. Research conducted at MAX IV, a Swedish national user facility, is supported by Vetenskapsrådet (Swedish Research Council, VR) under contract 2018-07152, Vinnova (Swedish Governmental Agency for Innovation Systems) under contract 2018-04969 and Formas under contract 2019-02496. The authors thanks A. E. Terry for the help during the SAXS measurements .

Supplementary material

Supplementary material associated with this article can be found in the online version at 10.1016/j.jcis.2026.140434.

References

[1] W.O. Baker, Microgel, a new macromolecule, Ind. Eng. Chem. 41 (3) (1949) 511–520. https://doi.org/10.1021/ie50471a016

[2] H. Staudinger, E. Husemann, Über hochpolymere verbindungen, 116. Mitteil.: Über das begrenzt quellbare poly–styrol, Berichte der deutschen chemischen Gesellschaft (A and B Ser.) 68 (8) (1935) 1618–1634. https://doi.org/10.1002/cber.19350680841

[3] B.R. Saunders, B. Vincent, Microgel particles as model colloids: theory, properties and applications, Adv. Colloid Interface Sci. 80 (1) (1999) 1–25. https://doi.org/10.1016/S0001-8686(98)00071-2

[4] T. Ngai, S.H. Behrens, H. Auweter, et al., Novel emulsions stabilized by pH and temperature sensitive microgels, Chem. Commun. (Cambridge, Engl.) (3) (2005) 331–333. https://doi.org/10.1039/b412330a

[5] M.A. Fernandez-Rodriguez, A. Martín-Molina, J. Maldonado-Valderrama, Microgels at interfaces, from mickering emulsions to flat interfaces and back, Adv. Colloid Interface Sci. 288 (2021) 102350. https://doi.org/10.1016/j.cis.2020.102350

[6] R. Pelton, Temperature-sensitive aqueous microgels, Adv. Colloid Interface Sci. 85 (1) (2000) 1–33. https://doi.org/10.1016/S0001-8686(99)00023-8

[7] D.M. Zhilin, A. Pich, Nano- and microgels: a review for educators, Chem. Teach. Int. 3 (2) (2021) 155–167. https://doi.org/10.1515/cti-2020-0008

[8] A. Scotti, M.F. Schulte, C.G. Lopez, J.J. Crassous, S. Bochenek, W. Richtering, How softness matters in soft nanogels and nanogel assemblies, Chem. Rev. 122 (13) (2022) 11675–11700.

[9] F. Scheffold, Pathways and challenges towards a complete characterization of microgels, Nat. Commun. 11 (1) (2020) 4315. https://doi.org/10.1038/s41467-020-17774-5

[10] J.E. Houston, L. Fruhner, A. de la Cotte, J. Rojo González, A.V. Petrunin, U. Gasser, R. Schweins, J. Allgaier, W. Richtering, A. Fernandez-Nieves, et al., Resolving the different bulk moduli within individual soft nanogels using small-angle neutron scattering, Sci. Adv. 8 (26) (2022) eabn6129.

[11] A.V. Petrunin, S. Bochenek, W. Richtering, A. Scotti, et al., Harnessing the polymer-particle duality of ultra-soft nanogels to stabilise smart emulsions, Phys. Chem. Chem. Phys. 25 (4) (2023) 2810–2820. https://doi.org/10.1039/D2CP02700C

[12] M. Rey, J. Kolker, J.A. Richards, I. Malhotra, T.S. Glen, N.Y.D. Li, F.H.J. Laidlaw, D. Renggli, J. Vermant, A.B. Schofield, S. Fujii, H. Löwen, P.S. Clegg, et al., Interactions between interfaces dictate stimuli-responsive emulsion behaviour, Nat. Commun. 14 (1) (2023) 6723. https://doi.org/10.1038/s41467-023-42379-z

[13] A. Maestro, D. Jones, C. Sánchez de Rojas Candela, E. Guzman, M.H.G. Duits, P. Cicuta, Tuning interfacial properties and processes by controlling the rheology and structure of poly(N-isopropylacrylamide) particles at air/water interfaces, Langmuir : ACS J. Surface. Colloid. 34 (24) (2018) 7067–7076. https://doi.org/10.1021/acs.langmuir.7b03879

[14] Z. Li, W. Richtering, T. Ngai, et al., Poly(N-isopropylacrylamide) microgels at the oil-water interface: temperature effect, Soft Matter 10 (33) (2014) 6182–6191. https://doi.org/10.1039/c4sm00888j

[15] M. Destribats, V. Lapeyre, E. Sellier, F. Leal-Calderon, V. Ravaine, V. Schmitt, Origin and control of adhesion between emulsion drops stabilized by thermally sensitive soft colloidal particles, Langmuir: ACS J. Surface. Colloid. 28 (8) (2012) 3744–3755.

[16] S. Stock, R. von Klitzing, Microgels at droplet interfaces of water-in-oil emulsions—challenges and progress, Curr. Opin. Colloid Interface Sci. 58 (2022) 101561. https://doi.org/10.1016/j.cocis.2021.101561

[17] X. Guan, H. Jiang, J. Lin, T. Ngai, Pickering emulsions: microgels as alternative surfactants, Curr. Opin. Colloid Interface Sci. 73 (2024) 101827. https://doi.org/10.1016/j.cocis.2024.101827

[18] I. Navarro Arrebola, L. Billon, G. Aguirre, Microgels self-assembly at liquid/liquid interface as stabilizers of emulsion: past, present & future, Adv. Colloid Interface Sci. 287 (2021) 102333. https://doi.org/10.1016/j.cis.2020.102333

[19] S. Tsuji, H. Kawaguchi, Thermosensitive pickering emulsion stabilized by poly(N-isopropylacrylamide)-carrying particles, Langmuir : ACS J. Surface. Colloid. 24 (7) (2008) 3300–3305. https://doi.org/10.1021/la701780g

[20] C. Monteux, C. Marlière, P. Paris, N. Pantoustier, N. Sanson, P. Perrin, et al., Poly(N-isopropylacrylamide) microgels at the oil-water interface: interfacial properties as a function of temperature, Langmuir: ACS J. Surface. Colloid. 26 (17) (2010) 13839–13846. https://doi.org/10.1021/la1019982

[21] M. Destribats, V. Lapeyre, M. Wolfs, E. Sellier, F. Leal-Calderon, V. Ravaine, V. Schmitt, et al., Soft microgels as pickering emulsion stabilisers: role of particle deformability, Soft Matter 7 (17) (2011) 7689. https://doi.org/10.1039/C1SM05240C

[22] Z. Li, K. Geisel, W. Richtering, T. Ngai, Poly(N-isopropylacrylamide) microgels at the oil–water interface: adsorption kinetics, Soft Matter 9 (41) (2013) 9939. https://doi.org/10.1039/C3SM52168K

[23] M. Destribats, M. Eyharts, V. Lapeyre, E. Sellier, I. Varga, V. Ravaine, V. Schmitt, et al., Impact of pNIPAM microgel size on its ability to stabilize pickering emulsions, Langmuir: ACS J. Surface. Colloid. 30 (7) (2014) 1768–1777. https://doi.org/10.1021/la4044396

[24] S. Backes, R. von Klitzing, Nanomechanics and nanorheology of microgels at interfaces, Polymers 10 (9) (2018) 1–23. https://doi.org/10.3390/polym10090978

[25] J. Harrer, M. Rey, S. Ciarella, H. Löwen, L.M.C. Janssen, N. Vogel, et al., Stimuli-responsive behavior of PNiPAm microgels under interfacial confinement, Langmuir: ACS J. Surface. Colloid. 35 (32) (2019) 10512–10521. https://doi.org/10.1021/acs.langmuir.9b01208

[26] S. Bochenek, A. Scotti, W. Ogieglo, M.Á. Fernández-Rodríguez, M.F. Schulte, R.A. Gumerov, N.V. Bushuev, I.I. Potemkin, M. Wessling, L. Isa, W. Richtering, et al., Effect of the 3D swelling of microgels on their 2D phase behavior at the liquid-liquid interface, Langmuir: ACS J. Surface. Colloid. 35 (51) (2019) 16780–16792. https://doi.org/10.1021/acs.langmuir.9b02498

[27] J. Liang, X. Xiao, T.-M. Chou, M. Libera, Analytical cryo-scanning electron microscopy of hydrated polymers and microgels, Acc. Chem. Res. 54 (10) (2021) 2386–2396. https://doi.org/10.1021/acs.accounts.1c00109

[28] K. Hrubanova, R. Skoupy, J. Nebesarova, F. Ruzicka, V. Krzyzanek, The sample preparation for cryo– SEM : the real ultrastructure of microbial biofilm or just artifacts?, in: European Microscopy Congress 2016: Proceedings, Wiley, 2016, pp. 203–204. https://doi.org/10.1002/9783527808465.EMC2016.6907

[29] C. Efthymiou, M.A.K. Williams, K.M. McGrath, Revealing the structure of high-water content biopolymer networks: diminishing freezing artefacts in cryo-SEM images, Food Hydrocolloid. 73 (2017) 203–212. https://doi.org/10.1016/j.foodhyd.2017.06.040

[30] K. Kuk, V. Abgarjan, L. Gregel, Y. Zhou, V. Carrasco Fadanelli, I. Buttinoni, M. Karg, et al., Compression of colloidal monolayers at liquid interfaces: in situ vs. ex situ investigation, Soft Matter 19 (2) (2023) 175–188. https://doi.org/10.1039/d2sm01125e

[31] A. Rubio-Andrés, D. Bastos-González, M.A. Fernandez-Rodriguez, In-situ characterization of microgel monolayers: controlling isostructural phase transitions for homogeneous crystal drying patterns, J. Colloid Interface Sci. 688 (2025) 328–340. https://doi.org/10.1016/j.jcis.2025.02.159

[32] H. Robertson, J. Zimmer, A.S. Name, C. Lux, S. Stock, R. von Klitzing, O. Soltwedel, In situ vs ex situ: comparing the structure of PNIPAM microgels at the air/water and air/solid interfaces, Soft Matter 22 (1) (2026) 127–138. https://doi.org/10.1039/D5SM00115C

[33] V. Abgarjan, K. Kuk, J.L.S. Garthe, T.L. Wigger, M. Karg, et al., Compression, expansion and relaxation of soft colloidal monolayers at the air/water interface, Soft Matter 21 (25) (2025) 5030–5044. https://doi.org/10.1039/d4sm01383b

[34] S. Bochenek, F. Camerin, E. Zaccarelli, A. Maestro, M.M. Schmidt, W. Richtering, A. Scotti, et al., In-situ study of the impact of temperature and architecture on the interfacial structure of microgels, Nat. Commun. 13 (1) (2022) 3744. https://doi.org/10.1038/s41467-022-31209-3

[35] J. Vialetto, S.N. Ramakrishna, L. Isa, In situ imaging of the three-dimensional shape of soft responsive particles at fluid interfaces by atomic force microscopy, Sci. Adv. 8 (45) (2022) eabq2019. https://doi.org/10.1126/sciadv.abq2019

[36] J. Kolker, J. Harrer, S. Ciarella, M. Rey, M. Ickler, L.M.C. Janssen, N. Vogel, H. Löwen, Interface-induced hysteretic volume phase transition of microgels: simulation and experiment, Soft Matter 17 (22) (2021) 5581-5589. https://doi.org/10.1039/d1sm00111f

[37] A. Armanious, Y. Gerelli, S. Micciulla, H.P. Pace, R.J.L. Welbourn, M. Sjöberg, B. Agnarsson, F. Höök, Probing the separation distance between biological nanoparticles and cell membrane mimics using neutron reflectometry with sub-nanometer accuracy, J. Am. Chem. Soc. 144 (45) (2022) 20726-20738. https://doi.org/10.1021/jacs.2c08456

[38] Y. Gerelli, G. Fragneto, Applications of Neutron Reflectometry to Soft Matter and Biological Systems, Elsevier, 2025, p. 669-700. https://doi.org/10.1016/b978-0-443-29116-6.00007-2

[39] Y. Gerelli, F. Camerin, S. Bochenek, M.M. Schmidt, A. Maestro, W. Richtering, E. Zaccarelli, A. Scotti, et al., Softness matters: effects of compression on the behavior of adsorbed microgels at interfaces, Soft Matter 20 (17) (2024) 3653–3665. https://doi.org/10.1039/D4SM00235K

[40] S. Bochenek, A. Scotti, W. Richtering, et al., Temperature-sensitive soft microgels at interfaces: air-water versus oil-water, Soft Matter 17 (4) (2021) 976–988. https://doi.org/10.1039/D0SM01774D

[41] J. Vialetto, N. Nussbaum, J. Bergfreund, P. Fischer, L. Isa, et al., Influence of the interfacial tension on the microstructural and mechanical properties of microgels at fluid interfaces, J. Colloid interface Sci. 608 (Pt 3) (2022) 2584–2592. https://doi.org/10.1016/j.jcis.2021.10.186

[42] D. Nečas, P. Klapetek, Gwyddion: an open-source software for SPM data analysis, Open Phys. 10 (1) (2012) 181–188. https://doi.org/10.2478/s11534-011-0096-2

[43] J.C. Crocker, D.G. Grier, Methods of digital video microscopy for colloidal studies, J. Colloid Interface Sci. 179 (1) (1996) 298–310. https://doi.org/10.1006/jcis.1996.0217

[44] M. Rey, M.Á. Fernández-Rodríguez, M. Steinacher, L. Scheidegger, K. Geisel, W. Richtering, T.M. Squires, L. Isa, et al., Isostructural solid-solid phase transition in monolayers of soft core-shell particles at fluid interfaces: structure and mechanics, Soft Matter 12 (15) (2016) 3545–3557. https://doi.org/10.1039/C5SM03062E

[45] FIGARO: The new horizontal neutron reflectometer at the ILL, Eur. Phys. J. Plus 126 (11) (2011) 1–22. https://doi.org/10.1140/epjp/i2011-11107-8

[46] Structure of surfactant and phospholipid monolayers at the air/water interface modeled from neutron reflectivity data, J. Colloid interface Sci. 531 (2018) 98–108. https://doi.org/10.1016/j.jcis.2018.07.022

[47] U. Gasser, J.S. Hyatt, J.-J. Lietor-Santos, E.S. Herman, L.A. Lyon, A. Fernandez-Nieves, Form factor of pNIPAM microgels in overpacked states, J. Chem. Phys. 141 (3) (2014) 034901. https://doi.org/10.1063/1.4885444

[48] S. Höfl, L. Zitzler, T. Hellweg, S. Herminghaus, F. Mugele, Volume phase transition of "smart" microgels in bulk solution and adsorbed at an interface: a combined AFM, dynamic light, and small angle neutron scattering study, Polymer 48 (1) (2007) 245–254. https://doi.org/10.1016/j.polymer.2006.10.026

[49] F. Camerin, M.Á. Fernández-Rodríguez, L. Rovigatti, M.-N. Antonopoulou, N. Gnan, A. Ninarello, L. Isa, E. Zaccarelli, Microgels adsorbed at liquid–liquid interfaces: a joint numerical and experimental study, ACS Nano 13 (4) (2019) 4548–4559.
[50] J.A. Henderson, R.W. Richards, J. Penfold, R.K. Thomas, J.R. Lu, Organization of poly(ethylene oxide) monolayers at the air-water interface, Macromolecules 26 (17) (1993) 4591-4600. https://doi.org/10.1021/ma00069a027
[51] T. Kawamoto, K. Yanagi, Y. Nishizawa, H. Minato, D. Suzuki, The compression of deformed microgels at an air/water interface, Chem. Commun. 59 (2023) 13289–13292.
[52] P.A. Kralchevsky, K. Nagayama, Capillary interactions between particles bound to interfaces, liquid films and biomembranes, Adv. Colloid Interface Sci. 85 (2–3) (2000) 145–192. https://doi.org/10.1016/S0001-8686(99)00016-0
[53] K. Kuk, J. Ringling, K. Gräff, S. Hänsch, V. Carrasco-Fadanelli, A.A. Rudov, I.I. Potemkin, R. von Klitzing, I. Buttinoni, M. Karg, Drying of soft colloidal films, Advanced science (Weinheim, Baden-Wurttemberg, Germany) 11 (47) (2024) e2406977. https://doi.org/10.1002/advs.202406977
[54] J. Zhang, R. Pelton, The dynamic behavior of poly(N-isopropylacrylamide) at the air/water interface, Colloid. Surface. A: Physicochemi. Eng. Aspect. 156 (1-3) (1999) 111-122. https://doi.org/10.1016/s0927-7757(99)00063-1
[55] L. Rovigatti, N. Gnan, A. Ninarello, E. Zaccarelli, Connecting elasticity and effective interactions of neutral microgels: the validity of the Hertzian model, Macromolecules 52 (13) (2019) 4895–4906.
[56] F. Camerin, N. Gnan, J. Ruiz-Franco, A. Ninarello, L. Rovigatti, E. Zaccarelli, Microgels at interfaces behave as 2D elastic particles featuring reentrant dynamics, Phys. Rev. X 10 (3) (2020) 031012.
[57] R. Rivas-Barbosa, F. Camerin, J. Vialetto, S.N. Ramakrishna, L. Isa, E. Zaccarelli, Comparing the structure of microgels at liquid-liquid and solid-liquid interfaces, Langmuir: ACS J. Surface. Colloid. 41 (25) (2025) 16674–16684. https://doi.org/10.1021/acs.langmuir.5c02599